TTF-Annulated Silicon Phthalocyanine Oligomers and Their External-Stimuli-Responsive Orientational Ordering

Shiina, Yuta
Department of Chemistry Graduate School of Science Tohoku University

Kage, Yuto
Department of Chemistry and Biochemistry Graduate School of Engineering, Kyushu University

Furukawa, Ko
Center for Coordination of Research Facilities Institute for Research Promotion Niigata University

Wang, Heng
School of Material and Chemical Engineering Zhengzhou University of Light Industry

他

出版情報：Angewandte Chemie International Edition. 59 (50), pp.22721-22730, 2020-12-01. Wiley
バージョン：

RESEARCH ARTICLE

TTF-Annulated Silicon Phthalocyanine Oligomers and Their External-Stimuli-Responsive Orientational Ordering

Yuta Shiina,[a] Yuto Kage,[b] Ko Furukawa,[c] Heng Wang,[d] Hirofumi Yoshikawa,[e] Hiroyuki Furuta,*[b] Nagao Kobayashi,*[a,f] and Soji Shimizu*[b]

[a] Y. Shiina, Prof. Dr. N. Kobayashi
Department of Chemistry, Graduate School of Science
Tohoku University
Sendai 980-8578 (Japan)
[b] Dr. Y. Kage, Prof. Dr. H. Furuta, Prof. Dr. S. Shimizu
Department of Chemistry and Biochemistry, Graduate School of Engineering and Center for Molecular Systems
Kyushu University
Fukuoka 819-0395 (Japan)
E-mail: hfuruta@cstf.kyushu-u.ac.jp, ssoji@cstf.kyushu-u.ac.jp
[c] Prof. Dr. K. Furukawa
Center for Coordination of Research Facilities, Institute for Research Promotion
Niigata University
Niigata 950-2181 (Japan)
[d] Dr. H. Wang
School of Material and Chemical Engineering
Zhengzhou University of Light Industry
Zhengzhou 450002 (P. R. China)
[e] Prof. Dr. H. Yoshikawa
School of Science and Technology
Kwansei Gakuin University
Hyogo 669-1337 (Japan)
[f] Prof. Dr. N. Kobayashi
Faculty of Textile Science and Technology
Shinshu University
Ueda 386-8567 (Japan)
E-mail: nagaok@shinshu-u.ac.jp

Supporting information for this article is given via a link at the end of the document.

Abstract: Orientational control of functional molecules is essential to create complex functionalities as seen in nature; however, such artificial systems have remained challenge. Herein, we succeeded in controlling rotational isomerism of μ-oxo silicon phthalocyanine (SiPc) oligomers to achieve an external-stimuli-responsive orientational ordering using intermolecular interactions of tetrathiafulvalene (TTF). In this system, three modes of orientations, free rotation, eclipsed conformation, and staggered conformation, were interconverted in response to the oxidation states of TTF, which varied interactions from association due to formation of mixed-valence TTF dimer to dissociation due to electrostatic repulsion between TTF dications. Furthermore, a stable performance of oligomers as a cathode material in a Li-ion battery proved that the one-dimensionally stacked, rotatable structure of SiPc oligomers is useful to control the orientation of functional molecules toward molecular electronics.

Introduction

μ-Oxo silicon phthalocyanine (SiPc) oligomers,[1] readily prepared by a dehydration reaction of axially hydroxy-substituted SiPc,[2] are a unique class of longitudinally stacked molecules (Figure 1a). Owing to the short distance of 3.3 Å between the SiPc layers,[3] peripheral substitution affects rotation of the SiPc units around the Si–O–Si axis; unsubstituted and β-alkyl-substituted SiPc oligomers exhibit free rotation in solution, whereas the rotational isomerism can be seen as a solvatochromism in the absorption spectra in the case of β-alkoxy-substituted SiPc oligomers.[4,5] Therefore, rotational behaviors of μ-oxo SiPc oligomers have been of significant interest because of their potential use as a molecular rotor to control orientation of functional molecules when attached to the periphery of the SiPc layers. Despite this expectation, control of rotational isomerism of μ-oxo SiPc oligomers has not yet been achieved.

To realize external-stimuli-responsive control of rotation of μ-oxo SiPc oligomers, we have designed herein periphery tetrathiafulvalene-annulated SiPc (TTF-SiPc) and its μ-oxo oligomers (Figure 1b). TTF[6,7] has been studied as an electron donor in its neutral state and as an organic semiconductor in its radical cation state.[8] By forming two aromatic 6π-electron 1,3-dithiolium cation structures from the overall nonaromatic 14π-electron neutral structure, TTF exhibits two reversible one-electron oxidation processes corresponding to the oxidation of the neutral state to its radical cation state ($TTF \rightarrow TTF^{\bullet+}$) and further to its dication state ($TTF^{\bullet+} \rightarrow TTF^{2+}$) (Figure 1c). When two TTF molecules are placed in close proximity, for example in a molecular cage or mechanically interlocked catenane,[9–12] there arises an intermolecular association interaction upon oxidation due to the formation of a mixed-valence dimer ($[TTF\text{-}TTF]^{\bullet+}$)[13,14] between a neutral TTF and a radical cation or a π-dimer ($TTF^{\bullet+}$-$TTF^{\bullet+}$)[13–15] between two radical cations. Further oxidation of the π-dimer can invert the interaction from association to dissociation due to electrostatic repulsion between two TTF dications (Figure 1d). These unique intermolecular interactions have been

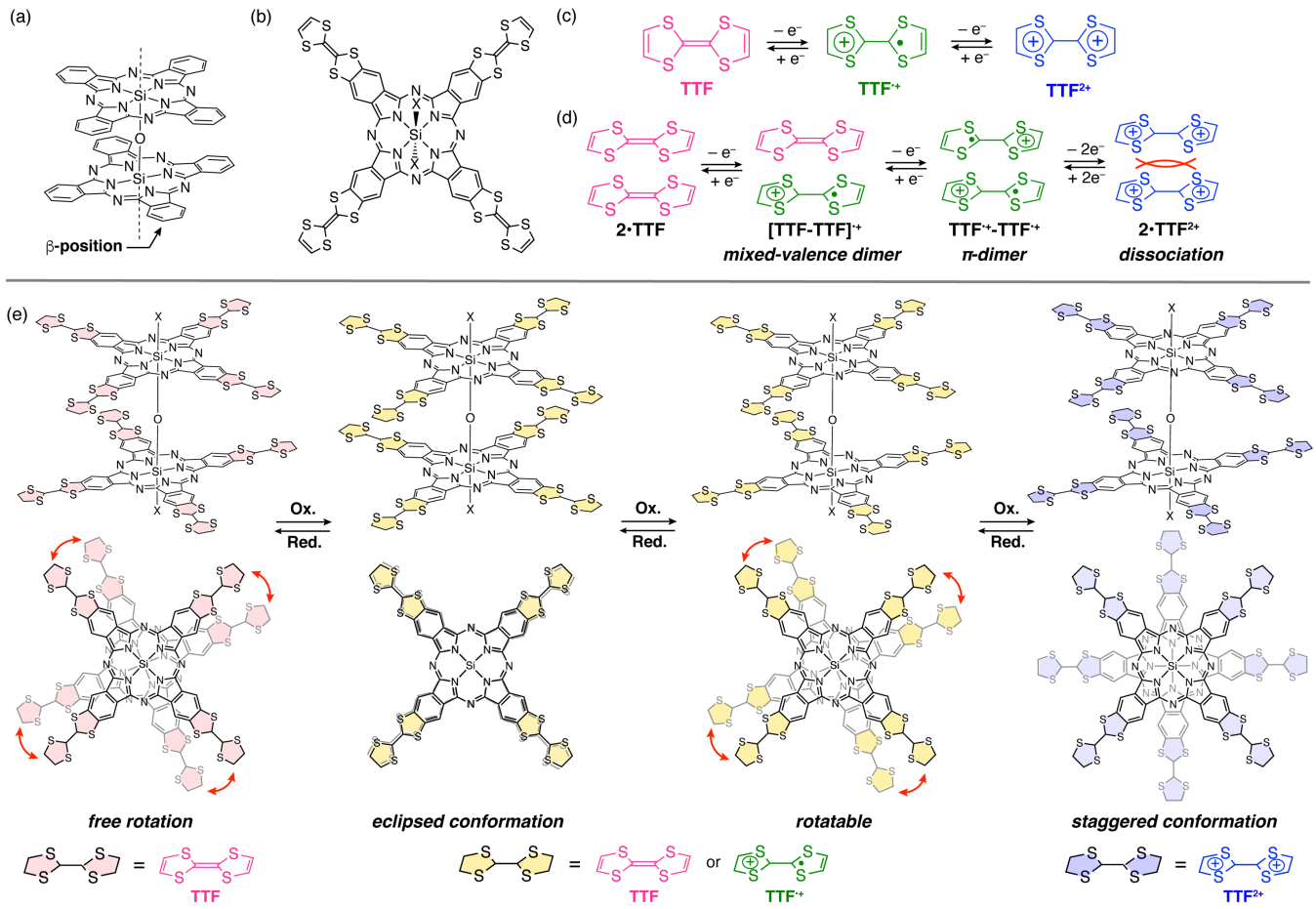

Figure 1. (a,b) Structures of μ-oxo SiPc oligomers (a constitutional dimer unit is shown) and TTF-SiPc. (c,d) TTF and interactions between two spatially proximate TTF molecules. (e) Redox-responsive behaviors of the conformation of **2mer**, top: side view, middle: top view, and bottom: corresponding oxidation states of TTF moieties.

used to establish molecular recognition systems and supramolecular architectures.[16–19]

In the current molecule, one-dimensionally stacked TTF units along the μ-oxo SiPc oligomers can function not only as a redox-active site but also as a switch to control the rotational isomerism of the μ-oxo SiPc oligomers by changing the interlayer interactions as depicted in Figure 1e. Proof-of-concept experiments on the external-stimuli-responsive orientational ordering of the SiPc units were demonstrated by means of electrochemistry, such as cyclic voltammetry and spectroelectrochemistry, using a dimer as the smallest model. Diagnostic UV/vis/NIR absorption bands revealed the oxidation states of TTF and the interlayer interactions arising from mixed-valence dimer and π-dimer formations or electrostatic repulsion between TTF dications. The interlayer interactions enabled orientational control of the SiPc units from free rotation to eclipsed conformation and further to staggered conformation. To investigate the importance of longitudinally stacked functional molecules and rotational motion in electronics applications, performances of TTF-SiPc and its μ-oxo oligomers for lithium-ion battery cathodes were examined. As a result of the multi-electron redox properties and the one-dimensional stacking of the TTF units, a mixture of μ-oxo oligomers exhibited a more stable cycle-life performance than that of the monomer.

Results and Discussion

A 1,3-diiminoisoindoline precursor (**TTF-In**) for the SiPc synthesis was prepared from TTF-annulated phthalonitrile (**TTF-Pn**).[20–22] TTF-SiPc with axial hydroxy ligands (**1mer-OH**) was synthesized from **TTF-In** using tetrachlorosilane as a template, followed by precipitation upon addition of methanol and water (Scheme 1). To prevent aggregation of **1mer-OH**, the axial hydroxy substituents were replaced with bulky triphenylsilyloxy groups to obtain TTF-SiPc monomer (**1mer**) in 39% yield from **TTF-In**. A mixture of the μ-oxo oligomers was obtained by refluxing a pyridine solution of **1mer-OH** for one day, followed by capping the terminal hydroxy groups with chlorotriphenylsilane (*Conditions A* in Scheme 1). The mixture was separated into oligomers from dimer to pentamer in moderate yields (**2mer**: 16%, **3mer**: 12%, **4mer-a**: 2.4% and **5mer**: 0.7%). **4mer-a** was contaminated with a trace amount of another rotational isomer (**4mer-b**). A prolonged reaction time of one week (*Conditions B* in Scheme 1) shifted the product distribution to higher oligomers: **2mer** (7.3%), **3mer** (9.2%),

4mer-a (trace), **4mer-b** (7.8%) and **5mer** (2.8%). MALDI-TOF-MS measurements on the reaction mixture after one week revealed molecular ion peaks corresponding to a series of oligomers up to octamer (Figure S1). In the UV/vis/NIR absorption spectra, the Q band of the SiPc moiety was observed at 712 nm for **1mer**, whereas the Q band was blue-shifted together with broadening and intensification upon μ-oxo oligomerization (**2mer**: 669 nm, **3mer**: 660 nm, **4mer-a**: 648 nm, **4mer-b**: 645 nm, and **5mer**: 642 nm, Figure S2). **4mer-b** exhibited an almost identical absorption spectrum to that of **4mer-a** (Figure S3).

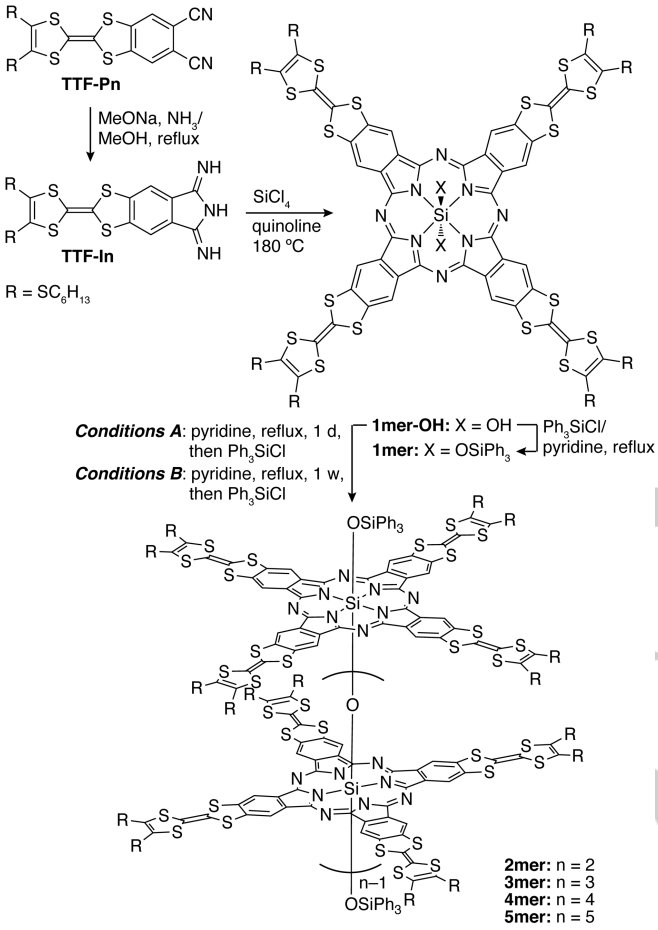

Scheme 1. Synthesis of TTF-SiPc and its μ-oxo oligomers.

The structure of **1mer** was unambiguously determined by single crystal X-ray diffraction analysis (Figure 2). As with conventional SiPc and neutral TTF, the SiPc moiety is highly planar, whereas the TTF moieties are slightly vaulted. The bulky triphenylsilyl groups cover the π-conjugated surface of the SiPc moiety to prevent π-π stacking. On the other hand, the TTF moieties form a crisscross stacking arrangement with S···S distances of 3.53–3.92 Å between the nearest neighbors (Figure S4).

Reflecting the fourfold symmetry of the TTF-SiPc moiety, **1mer** exhibited α-benzo protons of the SiPc moiety (α_H) as a singlet at 9.15 ppm and five thiohexyl proton signals at 2.94 (16H), 1.74 (16H), 1.49 (16H), 1.37 (32H), and 0.94 (24H) ppm (Figure 3a,c). Three proton signals observed for the triphenylsilyloxy groups at 6.78 (*para*), 6.39 (*meta*), and 4.85 (*ortho*) ppm indicated free rotation of the axial ligands in solution.

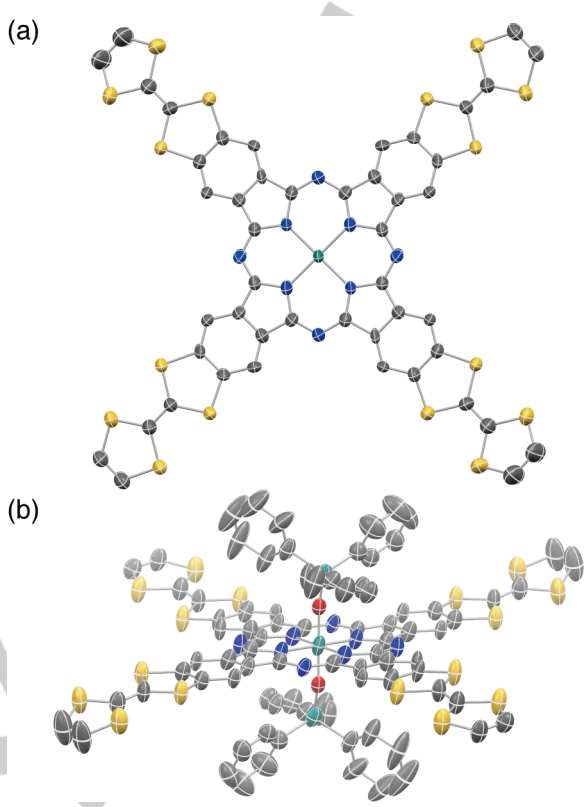

Figure 2. X-ray single crystal structure of **1mer**, (a) top and (b) side views. The thermal ellipsoids were scaled to the 50% probability level. Triphenylsilyloxy substituents in the top view and thiohexyl substituents and hydrogen atoms in both views were omitted for clarity.

The oligomers also exhibited simple ^{1}H NMR spectra (Figure 3b,c). The signal patterns of α_H and methylene protons adjacent to the sulfur atoms in thiohexyl groups (*S*-methylene proton: s_H) reflected the conformation of the SiPc moieties. **2mer** exhibited a single α_H signal at 8.80 ppm, whereas s_H signals were observed as two multiplets at 3.12 and 2.95 ppm due to the geminal and vicinal couplings arising from the nonequivalent environments between the interior and exterior protons (s_H^{INT} and s_H^{EXT}) in the sandwich structure of **2mer** (Figure 3d). In the case of **3mer**, the α_H signal appeared as a singlet at 8.47 and 8.34 ppm with an integral ratio of 1:2, which were assigned to the inside and outside α_H (α_H^{in} and α_H^{out}), respectively. The triplet signal at 3.13 ppm was assigned to s_H of the inside TTF-SiPc unit (s_H^{in}), whereas the interior and exterior s_H of the outside TTF-SiPc units ($s_H^{out\text{-}INT}$ and $s_H^{out\text{-}EXT}$) were resonated as two multiplets at 3.06 and 2.91 ppm, respectively (Figure 3d). The absence of geminal coupling for s_H^{in} indicates an equivalent environment around the inside TTF-SiPc unit. Compared with **1mer**, the α_H and triphenylsilyloxy proton signals gradually shifted upfield, whereas the s_H signals slightly shifted downfield due to the diatropic ring current effect of the neighboring SiPc units. Overall, these results reflect the free rotation of the TTF-SiPc units in **2mer** and **3mer** in solution at room temperature.

In contrast to **2mer** and **3mer**, rotational isomerism of the inner TTF-SiPc units at room temperature was observed for

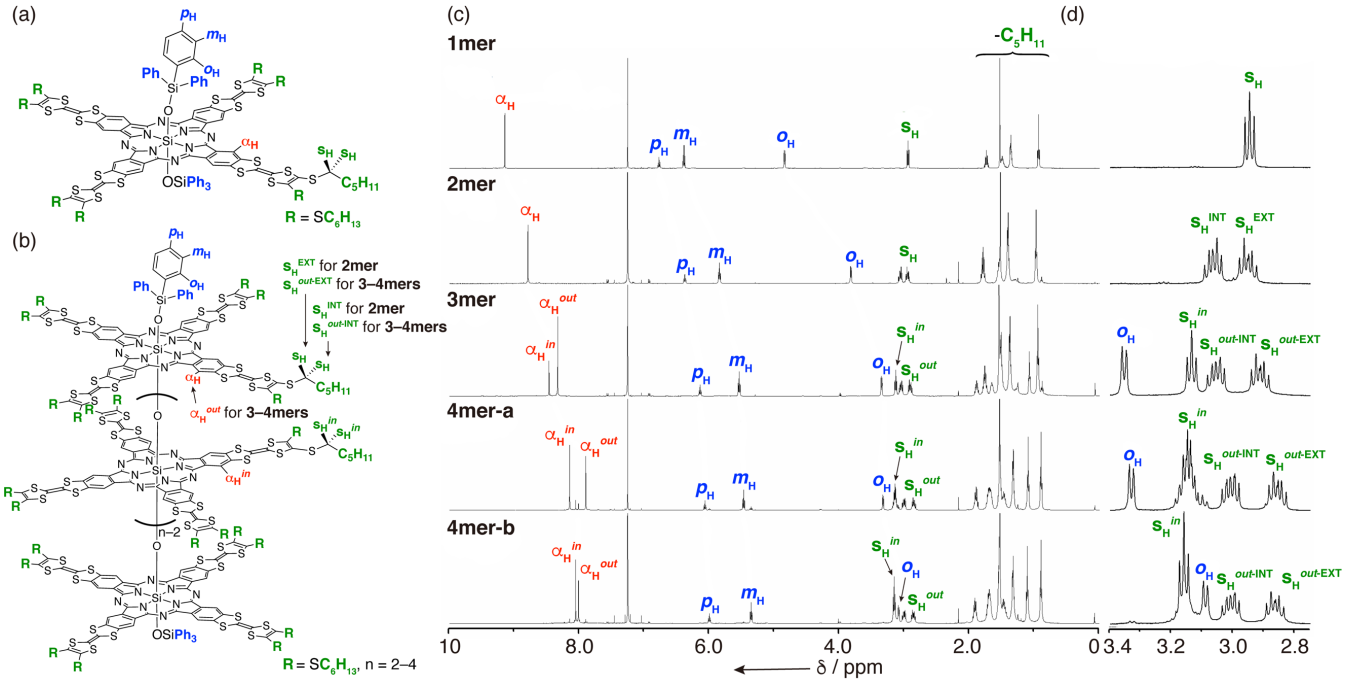

Figure 3. Structures of (a) **1mer** and (b) μ-oxo oligomers for the ^{1}H NMR assignment. (c) ^{1}H NMR spectra of **1mer** and μ-oxo oligomers (**2mer**–**4mer**) in $CDCl_3$ at room temperature. (d) Extended view of the area of the *S*-methylene protons. **αH**, **sH**, **oH**, ***m*H**, and ***p*H** denote α-benzo protons of the SiPc moieties, *S*-methylene protons of the TTF moieties, and *ortho*, *meta*, and *para* protons of the axial triphenylsilyloxy ligands, respectively.

higher oligomers (**4mer** (Figure 3) and **5mer** (Figure S5)). In the ^{1}H NMR spectrum of **4mer-a**, which was obtained after the μ-oxo oligomerization of **1mer-OH** in refluxing pyridine for one day (*Conditions A* in Scheme 1), the **αH** signals appeared at 8.15 and 7.91 ppm with an integral ratio of 1:1, and the **sH** signals were resonated at 3.15, 3.00, and 2.86 ppm with an integral ratio of 2:1:1. These proton signal patterns indicated differences between the two inside and two outside TTF-SiPc units. In addition, together with these major proton signals, minor signals were observed at 8.06, 8.02, 6.00, 5.36, and 3.09 ppm. After heating in pyridine for two days, these minor signals became intense to replace the major ones. Considering that an identical ^{1}H NMR spectrum was observed for **4mer-b** obtained from the μ-oxo oligomerization reaction for one week (*Conditions B* in Scheme 1), the minor signals in the ^{1}H NMR spectrum of **4mer-a** can be ascribed to **4mer-b**. The minor shifts and similar signal patterns of the outer **sH** of both **4mer-a** and **4mer-b** compared with those of **2mer** and **3mer** inferred free rotation of the two outside TTF-SiPc units at room temperature. In contrast, rather significant changes in the signal patterns of **αH** and inside **sH** reflected different environments of the inside TTF-SiPc units between **4mer-a** and **4mer-b**. Because only one **αH** signal was observed for the inside TTF-SiPc units in the case of both isomers, it can be presumed that the rotational angle between the inside TTF-SiPc units is fixed at 0° (eclipsed conformation) or 45° (staggered conformation) in a fourfold conformational symmetry.

To elucidate the conformations of oligomers in solution, chemical shifts of **αH** were calculated for the model structures using the GIAO method at the M06L/6-31G(d) level (Figures S6–S21). In the case of **2mer**, a single **αH** signal was calculated at 8.45 ppm for **2mer model-A** with the dihedral angle (θ) of 0º and 8.40 ppm for **2mer model-C** with θ of 45º, respectively, whereas two signals at 7.94 and 8.44 ppm were calculated for **2mer model-B** (θ = 22.5°) (Figure S19). Considering that the zero-point energies of **2mer model-A** and **-C** were 14.2 and 8.37 kcal/mol relative to that of **2mer model-B**, it can be presumed that the single **αH** signal observed for **2mer** is caused by free rotation of the SiPc units.

Because the single **αH** signal of **2mer** was reproduced by **2mer model-A** and **-C**, model structures with θ of 0° or 45° were used for the NMR calculations of **3mer** and **4mer**. In the case of both **3mer model-A** (θ1 = θ2 = 0º) and **-B** (θ1 = θ2 = 45º), the outer **αH** signal shifted upfield from those of the inside one (Figure S20). This agrees with the assignment of the observed signals based on the integral ratio. Similarly, in the case of **4mer**, the outside **αH** signal shifted upfield from the inside one (Figure S21). **4mer model-D** with all rotational angles of 45°exhibited the inside **αH** signal at 8.47 and 8.40 ppm and the outside ones at 7.58 and 7.53 ppm probably due to the highly deformed structure, in which diatropic ring current effects of neighboring SiPc units might be overestimated (Figure S17). The observed modest separation of the two **αH** signals ($\Delta\delta$) for **4mer-a** by 0.24 ppm and similar chemical shifts with $\Delta\delta$ of 0.04 ppm for **4mer-b** were reproduced with **4mer model-A** ($\Delta\delta$ = 0.28 ppm) or **-C** ($\Delta\delta$ = 0.30 ppm) and **4mer model-B** ($\Delta\delta$ = 0 ppm), respectively. These model structures also illustrate the difference in the signal pattern of the inside **sH** between **4mer-a** and **4mer-b**. The multiplet observed for **4mer-a** arises from geminal coupling due to the nonequivalent environments between the interior and exterior sides of the inside SiPc units in the eclipsed conformation of **4mer model-A** and **-C**. In contrast, the triplet signal of **4mer-b** indicates the absence of geminal coupling due to the staggered conformation in **4mer**

model-B. Variable-temperature NMR studies did not provide further information about the molecular dynamics because the intensities of all proton signals decreased due to the poor solubility at low temperature (Figures S22–S23). Although the possibility of thermally equilibrated fluctuation of the rotational angles at the NMR time scale cannot be excluded, it is more convincing to argue that the inside SiPc units in **4mer-a** and **4mer-b** are fixed at the eclipsed and staggered conformations, respectively. Since **4mer-b** was exclusively obtained after μ-oxo oligomerization for one week, **4mer-b** is a thermodynamic product, whereas **4mer-a** is a kinetic one. This assignment can also be rationalized from the sterically less hindered inside structure of **4mer-b** than **4mer-a**.

The cyclic voltammogram of **1mer** in *o*-dichlorobenzene (*o*-DCB) containing 0.1 M tetra-*n*-butylammonium perchlorate (TBAP) revealed two reversible oxidation waves at 0.13 and 0.44 V (vs Fc^+/Fc) and two reversible reduction waves at –1.18 and –1.72 V (Figure 4). According to previous reports,[1b,23] both oxidation couples can be ascribed to TTF-centered oxidation corresponding to a neutral state to a radical cation state (TTF → $TTF^{\bullet+}$) and further to a dication state ($TTF^{\bullet+}$ → TTF^{2+}), whereas the reduction waves can be assigned to SiPc-centered one-electron reductions. In comparison of the peak current intensities between the oxidation and reduction waves, each oxidation wave can be assumed to be a four-electron process, indicating the absence of interactions between TTF units through the SiPc moiety. The stepwise oxidation of **1mer** was also supported by the DFT calculations on neutral **1mer**, tetracation (**1mer**$^{4+}$), and octacation (**1mer**$^{8+}$) species at the M06L/6-31G(d) level (Figures 5, S6–S8, and S24–S26). The HOMO of **1mer** is quadruply degenerated and localized on the TTF moieties, whereas the doubly degenerate LUMO is centered on the SiPc moiety. **1mer**$^{4+}$ formed at the first oxidation has quadruply degenerate singly occupied molecular orbital (SOMO) and quadruply degenerate LUMO both localized on the TTF moieties, whereas the HOMO is localized on the SiPc moiety. Due to the removal of two electrons from each TTF unit, the LUMO of **1mer**$^{8+}$ is quadruply degenerate and localized on the TTF moieties.

In the case of **2mer** and **3mer**, two and three oxidation waves corresponding to the first TTF → $TTF^{\bullet+}$ oxidation process, were observed for **2mer** (–0.05 and 0.06 V) and **3mer** (–0.04, 0.11, and 0.23 V), respectively, whereas the $TTF^{\bullet+}$ → TTF^{2+} oxidation process was observed as a single oxidation wave with a large peak current (**2mer**: 0.38 V and **3mer**: 0.51 V, Figure 4). Considering the absence of interactions between the TTF units through the SiPc moiety in the case of **1mer**, the split TTF → $TTF^{\bullet+}$ oxidation process implies the presence of interlayer interactions due to mixed-valence dimer or π-dimer formation. Because of the interlayer interactions, the SiPc-centered reduction processes also split into multiple waves for **2mer** and **3mer** (**2mer**: –1.22, –1.51, and –1.93 V and **3mer**: –1.17, –1.42, –1.67, and –2.00 V). These assignments were also supported by DFT calculations, which revealed that multiply degenerate HOMO and LUMO are mainly localized on the TTF and SiPc moieties, respectively (Figures 5 and S27–S30). Despite the highly-lying SiPc-centered HOMO–8 of **3mer**, it is unlikely that the observed oxidation couples involve a SiPc-centered oxidation process because the HOMO–8 can be stabilized by the electron-deficient TTF cation moieties relative to the TTF-centered MOs (HOMO–9 – HOMO–12) during oxidation.

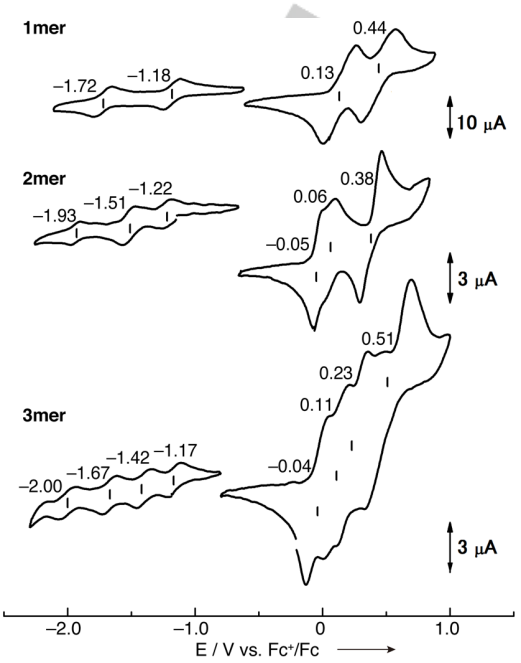

Figure 4. Cyclic voltammograms of **1mer**–**3mer** in *o*-DCB containing 0.1 M TBAP at a scan rate of 100 mV s^{-1} for **1mer** and 10 mV s^{-1} for **2mer** and **3mer**.

To give an insight into the observed electrochemical behaviors, spectroelectrochemcal measurements were performed on **1mer** and **2mer** (Figures 6 and 7). By applying a potential of 0.8 V vs Ag^+/Ag, which is slightly higher than the first oxidation potential of **1mer** at 0.13 V vs Fc^+/Fc, **1mer** exhibited absorptions at 439 and 797 nm in addition to a blue-shift and decrease of the Q band. These new bands are diagnostic absorption of TTF radical cation species.[14,24] The overall absorption spectral profile of **1mer**$^{4+}$ shown by the red line in Figure 6a can be regarded as an overlap of the absorption spectrum of the TTF radical cation and that of SiPc. Further oxidation at a higher potential (1.1 V vs Ag^+/Ag) than the second oxidation potential of **1mer** decreased the TTF radical cation absorption, indicating $TTF^{\bullet+}$ → TTF^{2+} oxidation. In addition, the Q band was intensified and red-shifted. In the absorption spectrum of **1mer**$^{8+}$ drawn by the red line in Figure 6b, the diagnostic absorption of a TTF dication species, which was reported to appear around 740 nm,[14,24] was not observed, and the overall absorption spectral profile resembles the absorption spectrum of regular SiPc.

The time-dependent (TD) DFT calculations at the M06L/6-31G(d) level explained the observed changes in the absorption spectra of **1mer** upon oxidation (Tables S1–S3). In all oxidation states, the main doubly degenerate bands around 650–660 nm (**1mer**: 662 nm (oscillator strength (*f*) = 0.86), **1mer**$^{4+}$: 654 nm (*f* = 0.81), and **1mer**$^{8+}$: 648 nm (*f* = 0.99)) comprise transitions from the SiPc-centered occupied MO (HOMO–4 for **1mer**, SOMO–4 (α-spin) and SOMO (β-spin) for **1mer**$^{4+}$, and HOMO for **1mer**$^{8+}$ in Figures S24–S26) to the doubly degenerate unoccupied,

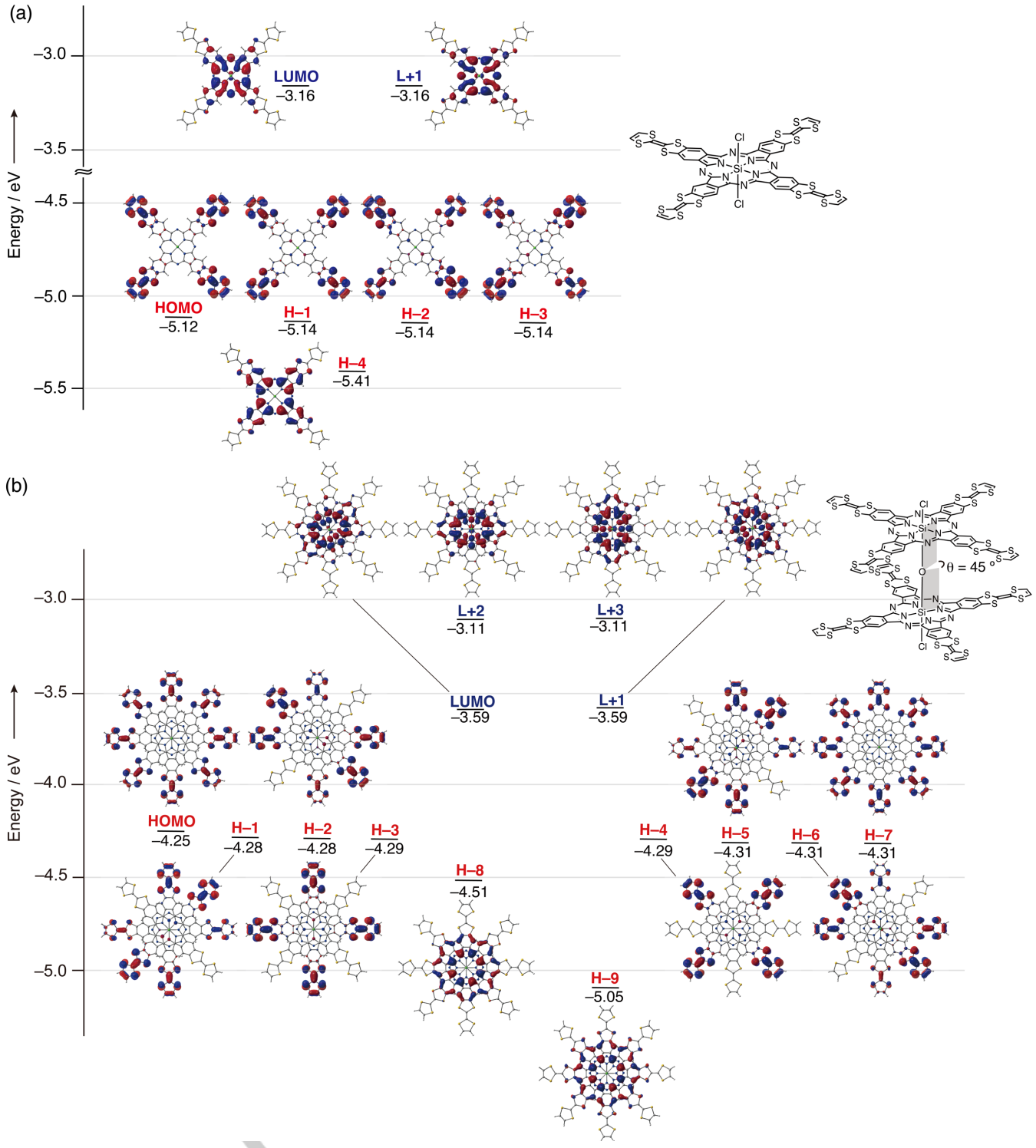

Figure 5. Partial frontier MO diagrams of (a) **1mer** and (b) **2mer** at the M06L/6-31G(d) level. The rotational angle of the SiPc units in **2mer** is 45°. Partial frontier MO diagrams of **2mer** including side views and **2mer** with other rotational angles (0° and 22.5°) are shown in Figures S27–S29. H and L denote the HOMO and LUMO, respectively.

SiPc-centered MOs (LUMO and LUMO+1 for **1mer**, LUMO and LUMO+1 (α-spin) and LUMO+4 and LUMO+5 (β-spin) for **1mer**$^{4+}$, and LUMO+4 and LUMO+5 for **1mer**$^{8+}$). Therefore, the observed intense bands with an absorption maximum at 715 nm for **1mer**, 702 nm for **1mer**$^{4+}$, and 718 nm for **1mer**$^{8+}$ can be assigned as the Q band of the SiPc moiety. This result indicates that the electronic structure of the SiPc moiety remained intact upon oxidation.

The TDDFT calculations also revealed TTF-origin bands in the Q band region although the transition energies were not perfectly reproduced. Doubly degenerate bands of **1mer** with forbidden nature at 797 nm (f = 0.06) comprise transitions from the TTF-centered HOMO to the doubly degenerate SiPc-centered LUMO. These bands presumably overlap to broaden the Q band of **1mer**. Doubly degenerate TTF-centered absorption of **1mer^{4+}** at 673 nm with f = 0.17 due to the transition from doubly degenerate SOMO–1 and SOMO–2 for β-spin to one of the quadruply degenerate LUMO can be assigned to the radical cation absorption of the TTF moieties at 797 nm in the absorption spectrum of **1mer^{4+}**. TTF-centered transitions of **1mer^{8+}** at 524 nm arising from the HOMO–1 and HOMO–2 to the LUMO+2 (f = 0.39) are probably hidden within the shorter-wavelength edge of the Q band in the absorption spectrum of **1mer^{8+}**.

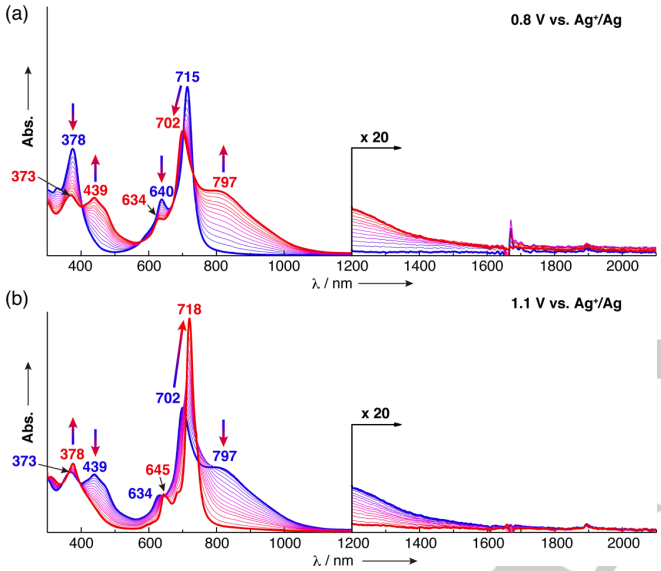

Figure 6. UV/vis/NIR spectroelectrochemistry of **1mer** in *o*-DCB containing 0.3 M TBAP by applying potentials of (a) 0.8 and (b) 1.1 V vs Ag^+/Ag.

In the spectroelectrochemistry of **2mer**, by applying a potential of 0.65 V vs Ag^+/Ag, which corresponds to the first oxidation to the tetracation species (**2mer^{4+}**), broad absorption around 1850 nm appeared in addition to the TTF radical cation absorption at 785 nm (Figure 7a). This NIR band is diagnostic for a mixed-valence dimer species.[13] Furthermore, the Q band was slightly blue-shifted to 662 nm. These absorption spectral changes were caused by forming an eclipsed conformation of the SiPc units, allowing the interlayer formation of mixed-valence dimers of TTF (Figure 1e). At the second oxidation potential (0.76 V vs Ag^+/Ag), which corresponds to **2mer^{4+}** → **2mer^{8+}** oxidation, the NIR band decreased, while the TTF radical cation absorption at 785 nm split into an intense band at 727 nm and a shoulder-like band at 933 nm. In addition, the Q band decreased in intensity together with a decent blue-shift by 5 nm. According to a report on a face-to-face TTF dimer,[14] which ascribed a similar Davydov splitting of TTF radical cation absorption to π-dimer formation, the observed changes imply the presence of π-dimer species. Further oxidation at 1.25 V vs Ag^+/Ag, which is higher than the third oxidation potential of **2mer**, resulted in decreases of the TTF-radical cation absorptions, whereas the Q band was intensified together with a red-shift by 33 nm. The absorption spectrum of the electrochemically generated hexadecacation species (**2mer^{16+}**) shown by the red line in Figure 7c is similar to that of **1mer^{8+}** with a blue-shift of the Q band by 28 nm. The TDDFT calculations on model structures of **2mer** (**2mer model-A–C**) revealed that the Q band spectral profiles can vary depending on the rotational angles (Tables S4–S6). Compared with **1mer**, **2mer model-A–C** exhibited a splitting of the Q-band into intense blue-shifted bands and weak red-shifted bands. In the case of **2mer model-A** (θ = 0°) and **-C** (θ = 45°), the oscillator strengths of the doubly degenerate weak bands are 0.01 or less due to their symmetry forbidden nature (**2mer model-A**: 867 nm (f = 0.01) and **2mer model-C**: 867 nm (f = 0.003)). In contrast, six Q-band-origin weak bands were predicted for **2mer model-B** (θ = 22.5°). Consequently, these TDDFT calculations indicate that free rotation of the SiPc units broadens the Q band of **2mer**, whereas a fixed eclipsed or staggered conformation causes a sharp Q band. The same discussion can be applied to **2mer^{16+}** because the electronic structure of the SiPc moieties remains intact according to the above-mentioned discussion on the Q band of **1mer^{8+}**. Considering the electrostatic repulsion between the TTF dications, the observed sharp Q band of **2mer^{16+}** indicates its staggered conformation (Figure 1e).

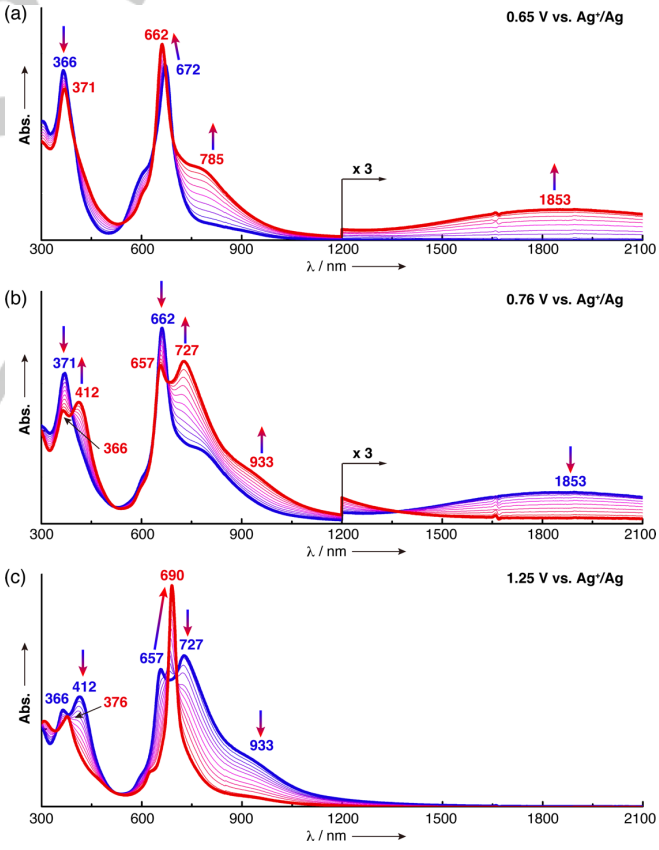

Figure 7. UV/vis/NIR spectroelectrochemistry of **2mer** in *o*- DCB containing 0.3 M TBAP by applying potentials of (a) 0.65, (b) 0.76, and (c) 1.25 V vs Ag^+/Ag.

The electrochemical ESR studies on **1mer** and **2mer** further shed light on the electronic structures in each oxidation state. In the case of **1mer**, a symmetric derivative curve without hyperfine structures gradually increased by applying potentials up to 0.7 V

vs Ag^+/Ag (Figure 8a,c). According to previous reports on benzo- and heteroaromatic ring-fused TTF analogs,[25,26] the observed ESR signal is ascribed to the TTF-centered radical species with a spin delocalized nature. This also indicates the absence of spin-spin interactions of TTF radicals through the SiPc core. Further oxidation at a higher potential than the second oxidation couple decreased the ESR signal because of the formation of ESR-silent **1mer^{8+}**.

In the case of **2mer**, a similar ESR signal increased, and the intensity profile showed a local maximum at the first oxidation potential (0.5 V vs Ag^+/Ag) (Figure 8b,d). At higher potentials, the intensities further increased to a maximum at the second oxidation potential and then decreased to become silent at the third oxidation potential. Because of the spin-coupling, a π-dimer is ESR-silent.[9,14] The observed ESR intensity profiles of **2mer** looked contradictory to the presumed formation of π-dimer species based on the spectroelectrochemistry. This can be rationalized considering the one order of magnitude lower equilibrium constant of the π-dimer formation (0.6 M^{-1} in acetone) compared with that of mixed-valence dimer formation (6.0 M^{-1} in dichloromethane).[13] The slight decrease in the ESR intensity after the first oxidation potential indicates a π-dimer formation in the eclipsed conformation maintained by the attractive forces due to the mixed-valence dimer species. When the number of π-dimer species increases, the attractive force becomes too weak to maintain the eclipsed conformation. The constant increase in ESR intensities up to the second oxidation potential implies a shift of equilibrium from the eclipsed conformation to the rotatable state as depicted in Figure 1e.

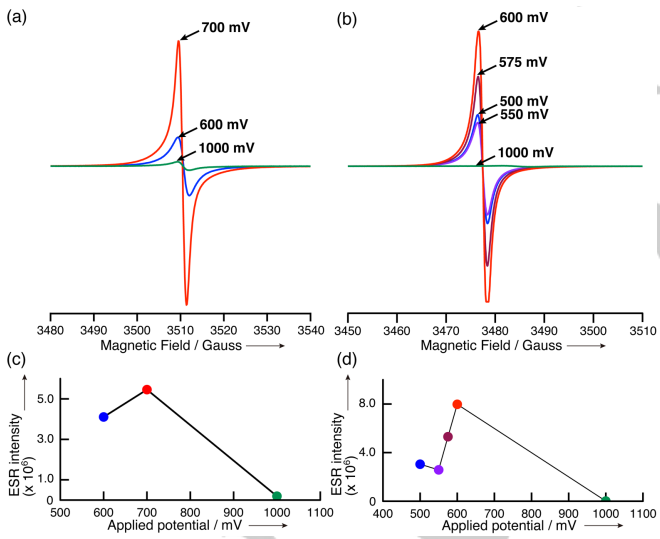

Figure 8. Electrochemical ESR spectra of (a) **1mer** and (b) **2mer** in *o*-DCB (0.5 mM) containing 0.3 M TBAP by applying potentials vs Ag^+/Ag. Plots of the ESR intensities versus applied potentials for (c) **1mer** and (d) **2mer**.

To elucidate the effect of the longitudinal stacking of TTF on electronics applications, we investigated lithium-ion battery cathode performance using **1mer-OH** or a mixture of μ-oxo oligomers (**oligomer-OH**). **oligomer-OH** with axial hydroxy ligands was obtained by refluxing **1mer-OH** in pyridine. The components of the mixture were determined to be 12% of **1mer-OH**, 38% of **2mer-OH**, 37% of **3mer-OH**, 13% of **4mer-OH** and a trace of **5mer-OH** based on the integral ratios of proton signals in the ^1H NMR spectrum. The fabricated coin cells were composed of a Li metal foil anode, a cathode containing 10wt% of **1mer-OH** or **oligomer-OH**, 20wt% of polyvinylidene fluoride, and 70 wt% of carbon black, and an electrolyte solution of $LiPF_6$ in ethylene carbonate/diethylene carbonate.

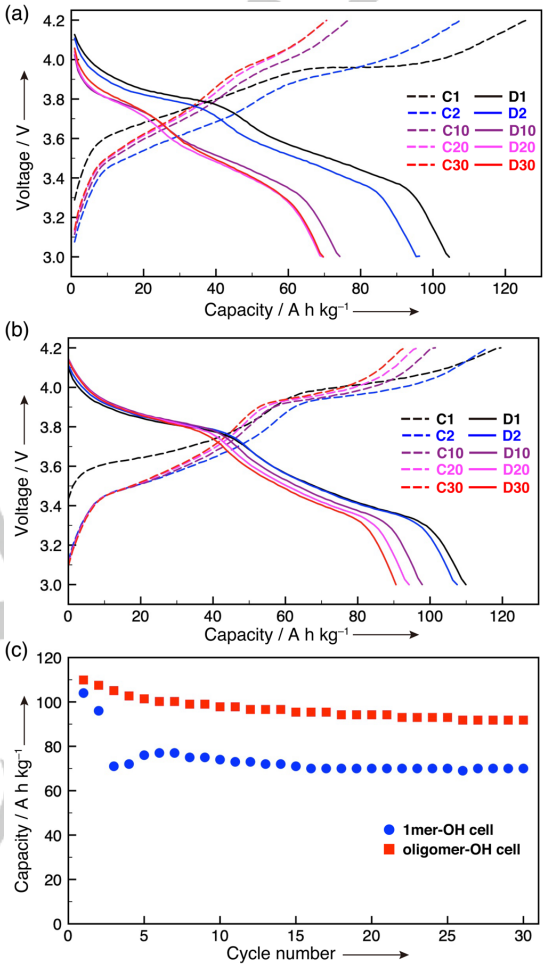

Figure 9. Selected charge/discharge curves of (a) **1mer-OH** cell and (b) **oligomer-OH** cell and (c) cycle performance for 30 discharge process cycles. **Cn** and **Dn** (n = 1, 2, 10, 20, and 30) in (a) and (b) denote the *n*th cycle of charge and discharge processes, respectively.

The charge/discharge curves were measured at a constant current of 1 mA in the voltage range of 3.0–4.2 V (Figure 9a,b). The capacities of **1mer-OH** and **oligomer-OH** were normalized by their weights. Both cells exhibited reproducible charge/discharge cycles after the second cycle. The initial charge voltage was 3.3 V vs Li^+/Li. Two voltage plateaus at around 3.4 and 3.8 V correspond to the first and second oxidation of the TTF moieties, and no significant split of the first oxidation process was observed for **oligomer-OH**. The first charge capacities were 108 and 118 A h kg^{-1} for the **1mer-OH** and **oligomer-OH** cells, which agree with the theoretical charge capacities of 97 and 98 A h kg^{-1}, respectively. After 30 cycles, the capacity of the **1mer-OH** cell decreased to 67%, whereas the capacity of **oligomer-OH** cell was maintained at 84% (Figure 9c). This noteworthy improvement of cycle performance upon oligomerization indicates an importance

of the longitudinally stacked structure, which enables efficient charge transportation and prevents dissolution of charged species into the electrolyte.

Conclusion

In summary, we have succeeded in controlling rotational isomerism of SiPc oligomers for the first time using intermolecular interactions of TTF, and the proof-of-concept investigation by electrochemistry revealed the external-stimuli-responsive orientational ordering of the dimer. In this molecular system, the interlayer association forces arising from the formations of mixed-valence TTF dimer and π-dimer and dissociation force due to the electrostatic repulsion between TTF dications enabled the orientational control of the SiPc units from the free rotation to the eclipsed conformation and further to the staggered conformation. Furthermore, the longitudinal stacking of TTF units improved the charge/discharge cycle performance as a cathode-active material in a lithium-ion battery by 25%. With these results in hand, we anticipate that TTF-SiPc and its μ-oxo oligomers can be applied to photovoltaics and field effect transistors. Moreover, the current molecular design based on the periodically stacked μ-oxo SiPc oligomers also allows the arrangement of not only TTF but also other types of functional molecules. Research along these directions can open advanced artificial molecular systems for efficient photon energy harvesting and energy and electron transfer.

Acknowledgments

This work was supported by Grants-in-Aids from JSPS (No. JP19H02703 and JP15H00756).

Conflict of interest

The authors declare no conflict of interest.

Keywords: phthalocyanine • tetrathiafulvalene • supramolecular chemistry • orientational ordering • lithium-ion battery

[1] a) J. N. Esposito, J. E. Lloyd, M. E. Kenney, *Inorg. Chem.* **1966**, *5*, 1979-1984; b) D. W. DeWulf, J. K. Leland, B. L. Wheeler, A. J. Bard, D. A. Batzel, D. R. Dininny, M. Kenney, *Inorg. Chem.* **1987**, *26*, 266-270.

[2] R. D. Joyner, M. E. Kenney, *Inorg. Chem.* **1962**, *1*, 236-238.

[3] a) Y. Yang, V. O. Kennedy, J. B. Updegraph III, B. Samas, D. Macikenas, B. Chaloux, J. A. Miller, E. M. Van Goethem, M. E. Kenney, *J. Phys. Chem. A* **2012**, *116*, 8718-8730; b) Y. Yang, B. Samas, V. O. Kennedy, D. Macikenas, B. L. Chaloux, J. A. Miller, R. L. Speer Jr., J. Protasiewicz, A. A. Pinkerton, M. E. Kenney, *J. Phys. Chem. A* **2011**, *115*, 12474-12485.

[4] J. Kleinwachter, M. Hanack, *J. Am. Chem. Soc.* **1997**, *119*, 10684-10695.

[5] K. Oniwa, S. Shimizu, Y. Shiina, T. Fukuda, N. Kobayashi, *Chem. Commun.* **2013**, *49*, 8341-8343.

[6] F. Wudl, G. M. Smith, E. J. Hufnagel, *J. Chem. Soc. D: Chem. Commun.* **1970**, 1453-1454.

[7] S. Hünig, G. Kießlich, D. Scheutzow, R. Zahradnik, P. Carsky, *Int. J. Sulfur Chem., Part C* **1971**, *6*, 109.

[8] a) F. Wudl, D. Wobschall, E. J. Hufnagel, *J. Am. Chem. Soc.* **1972**, *94*, 670-672; b) M. Bendikov, F. Wudl, D. F. Perepichka, *Chem. Rev.* **2004**, *104*, 4891-4945.

[9] A. Y. Ziganshina, Y. H. Ko, W. S. Jeon, K. Kim, *Chem. Commun.* **2004**, *20*, 806-807.

[10] M. Yoshizawa, K. Kumazawa, M. Fujita, *J. Am. Chem. Soc.* **2005**, *127*, 13456-13457.

[11] a) J. M. Spruell, A. Coskun, D. C. Friedman, R. S. Forgan, A. A. Sarjeant, A. Trabolsi, A. C. Fahrenbach, G. Barin, W. F. Paxton, S. K. Dey, M. A. Olson, D. Benítez, E. Tkatchouk, M. T. Colvin, R. Carmielli, S. T. Caldwell, G. M. Rosair, S. G. Hewage, F. Duclairoir, J. L. Seymour, A. M. Z. Slawin, W. A. Goddard III, M. R. Wasielewski, G. Cooke, J. F. Stoddart, *Nat. Chem.* **2010**, *2*, 870-879; b) M. Frasconi, T. Kikuchi, D. Cao, Y. Wu, W.-G. Liu, S. M. Dyar, G. Barin, A. A. Sarjeant, C. L. Stern, R. Carmieli, C. Wang, M. R. Wasielewski, W. A. Goddard III, J. F. Stoddart, *J. Am. Chem. Soc.* **2014**, *136*, 11011-11026; c) A. Coskun, J. M. Spruell, G. Barin, A. C. Fahrenbach, R. S. Forgan, M. T. Colvin, R. Carmieli, D. Benítez, E. Tkatchouk, D. C. Friedman, A. A. Sarjeant, M. R. Wasielewski, W. A. Goddard III, J. F. Stoddart, *J. Am. Chem. Soc.* **2011**, *133*, 4538-4547.

[12] a) M. Fumanal, M. Capdevila-Cortada, J. S. Miller, J. J. Novoa, *J. Am. Chem. Soc.* **2013**, *135*, 13814-13826; b) P.-T. Chiang, N.-C. Chen, C.-C. Lai, S.-H. Chiu, *Chem. Eur. J.* **2008**, *14*, 6546-6552.

[13] S. V. Rosokha, J. K. Kochi, *J. Am. Chem. Soc.* **2007**, *129*, 828-838.

[14] M. Hasegawa, K. Daigoku, K. Hashimoto, H. Nishikawa, M. Iyoda, *Bull. Chem. Soc. Jpn.* **2012**, *85*, 51-60.

[15] V. Khodorkovsky, L. Shapiro, P. Krief, A. Shames, G. Mabon, A. Gorgues, M. Giffard, *Chem. Commun.* **2001**, *29*, 2736-2737.

[16] a) A. Jana, S. Bähring, M. Ishida, S. Goeb, D. Canevet, M. Sallé, J. O. Jeppesen, J. L. Sessler, *Chem. Soc. Rev.* **2018**, *47*, 5614-5645; b) A. Jana, M. Ishida, J. S. Park, S. Bähring, J. O. Jeppesen, J. L. Sessler, *Chem. Rev.* **2017**, *117*, 2641-2710.

[17] D. Canevet, M. Sallé, G. Zhang, D. Zhang, D. Zhu, *Chem. Commun.* **2009**, 2245-2269.

[18] a) J. O. Jeppesen, M. B. Nielsen, J. Becher, *Chem. Rev.* **2004**, *104*, 5115-5132; b) M. B. Nielsen, C. Lomholt, J. Becher, *Chem. Soc. Rev.* **2000**, *29*, 153-164.

[19] M. Hasegawa, M. Iyoda, *Chem. Soc. Rev.* **2010**, *39*, 2420-2429.

[20] a) C. Loosli, C. Jia, S.-X. Liu, M. Haas, M. Dias, E. Levillain, A. Neels, G. Labat, A. Hauser, S. Decurtins, *J. Org. Chem.* **2005**, *70*, 4988-4992; b) C. A. Donders, S.-X. Liu, C. Loosli, L. Sanguinet, A. Neels, S. Decurtins, *Tetrahedron* **2006**, *62*, 3543-3549.

[21] a) T. Kimura, D. Watanabe, T. Namauo, *Heteroatom Chem.* **2011**, *22*, 605-611; b) T. Kimura, *HETEROCYCLES* **2013**, *87*, 245-274.

[22] M. Kimura, S. Otsuji, J. Takizawa, Y. Tatewaki, T. Fukawa, H. Shirai, *Chem. Lett.* **2010**, *39*, 812-813.

[23] S. Shimizu, Y. Yamazaki, N. Kobayashi, *Chem. Eur. J.* **2013**, *19*, 7324-7327.

[24] K.-i. Nakamura, T. Takashima, T. Shirahata, S. Hino, M. Hasegawa, Y. Mazaki, Y. Misaki, *Org. Lett.* **2011**, *13*, 3122-3125.

[25] C. Bejger, C. M. Davis, J. S. Park, V. M Lynch, J. B. Love, J. L. Sessler, *Org. Lett.* **2011**, *13*, 4902-4905.

[26] M. Takase, N. Yoshida, T. Nishinaga, M. Iyoda, *Org. Lett.* **2011**, *13*, 3896-3899.

Entry for the Table of Contents

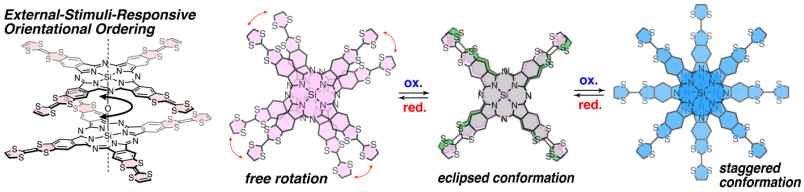

External-stimuli-responsive orientational ordering was achieved based on the rotational isomerism of μ-oxo silicon phthalocyanine oligomers and intermolecular interaction of tetrathiafulvalene. The stable performance of oligomers as a lithium-ion battery cathode compared with monomer ensures potential use of one-dimensionally stacked oligomer structures toward creation of artificial molecular systems for energy/electron harvesting and transfer.